

# A single-molecule force spectroscopy nanosensor for the identification of new antibiotics and antimalarials

Xavier Sisquella,\* Karel de Pourcq,<sup>†</sup> Javier Alguacil,<sup>‡</sup> Jordi Robles,<sup>‡</sup> Fausto Sanz,<sup>§</sup> Dario Anselmetti,<sup>#</sup> Santiago Imperial,<sup>†,||</sup> and Xavier Fernández-Busquets<sup>||,\*\*,1</sup>

\*Nanotechnology Platform, Barcelona Science Park, Barcelona, Spain; <sup>†</sup>Department of Biochemistry and Molecular Biology, <sup>‡</sup>Department of Organic Chemistry, <sup>§</sup>Department of Physical Chemistry, and <sup>||</sup>Biomolecular Interactions Team, Nanoscience and Nanotechnology Institute, University of Barcelona, Barcelona, Spain; <sup>#</sup>Experimental Biophysics and Applied Nanoscience, Bielefeld University, Bielefeld, Germany; and <sup>\*\*</sup>Nanobioengineering Group, Institute for Bioengineering of Catalonia, Barcelona, Spain

**ABSTRACT** An important goal of nanotechnology is the application of individual molecule handling techniques to the discovery of potential new therapeutic agents. Of particular interest is the search for new inhibitors of metabolic routes exclusive of human pathogens, such as the 2-C-methyl-D-erythritol-4-phosphate (MEP) pathway essential for the viability of most human pathogenic bacteria and of the malaria parasite. Using atomic force microscopy single-molecule force spectroscopy (SMFS), we have probed at the single-molecule level the interaction of 1-deoxy-D-xylulose 5-phosphate synthase (DXS), which catalyzes the first step of the MEP pathway, with its two substrates, pyruvate and glyceraldehyde-3-phosphate. The data obtained in this pioneering SMFS analysis of a bisubstrate enzymatic reaction illustrate the substrate sequentiality in DXS activity and allow for the calculation of catalytic parameters with single-molecule resolution. The DXS inhibitor fluoropyruvate has been detected in our SMFS competition experiments at a concentration of 10  $\mu$ M, improving by 2 orders of magnitude the sensitivity of conventional enzyme activity assays. The binding of DXS to pyruvate is a 2-step process with dissociation constants of  $k_{\text{off}} = 6.1 \times 10^{-4} \pm 7.5 \times 10^{-3}$  and  $1.3 \times 10^{-2} \pm 1.0 \times 10^{-2} \text{ s}^{-1}$ , and reaction lengths of  $x_p = 3.98 \pm 0.33$  and  $0.52 \pm 0.23 \text{ \AA}$ . These results constitute the first quantitative report on the use of nanotechnology for the biodiscovery of new antimalarial enzyme inhibitors and open the field for the identification of compounds represented only by a few dozens of molecules in the sensor chamber.—Sisquella, X., de Pourcq, K., Alguacil, J., Robles, J., Sanz, F., Anselmetti, D., Imperial, S., Fernández-Busquets, X. A single-molecule force spectroscopy nanosensor for the identification of new antibiotics and antimalarials. *FASEB J.* 24, 4203–4217 (2010). [www.fasebj.org](http://www.fasebj.org)

**Key Words:** malaria • 2-C-methyl-D-erythritol-4-phosphate pathway • 1-deoxy-D-xylulose 5-phosphate synthase • pyruvate • glyceraldehyde-3-phosphate • drug discovery

MICROBIAL DISEASES HAVE EVOLVED strong and devastating resistance to many antibiotics, a process occur-

ring at low levels in natural populations but that can become common within a few years of the commercial adoption of a new drug (1). The urgent need for new efficient compounds for the treatment of disease has stimulated the development of strategies addressed to their identification (2). The corresponding therapeutic targets must be, of preference, molecules that take part in essential and exclusive processes of the pathogens and that, therefore, do not exert pernicious side effects on the host organism. The biosynthesis of isoprenoids, such as sterols and ubiquinones, depends on the condensation of different numbers of isopentenyl diphosphate (IPP) units (3). In archaea, fungi, and animals, IPP is derived from the mevalonate pathway (Fig. 1A). In contrast, in most bacteria, algae, and in the chloroplasts of plants, IPP is synthesized by the mevalonate-independent 2-C-methyl-D-erythritol-4-phosphate (MEP) pathway (4). The MEP pathway (Fig. 1B) begins with the thiamine pyrophosphate (TPP)-dependent condensation of glyceraldehyde-3-phosphate (G3P) and pyruvate to yield 1-deoxy-D-xylulose 5-phosphate (DXP), a step catalyzed by DXP synthase (DXS) (5). Whereas the MEP pathway is absent in mammals, it is essential for most human bacterial pathogens (6), and thus its enzymes are attractive targets for the development of novel antibiotics (7). The MEP pathway has also been identified in the apicoplast, a relict chloroplast of *Plasmodium falciparum* and related parasites, where it plays an essential function for their survival (8, 9).

Although the application of nanotechnology in the life sciences, nanobiotechnology, is starting to have an effect in drug discovery and development (10), this new area of study has only had a very limited infiltration in the research related to certain diseases specially prevalent in developing countries. Regarding malaria, the concept of nanotechnology is almost exclusively applied to the use of nanoparticles for targeted drug delivery (11); to date not

<sup>1</sup> Correspondence: Nanobioengineering Group, Institute for Bioengineering of Catalonia, Baldiri Reixac 10-12, Barcelona E08028, Spain. E-mail: [xfernandez\\_busquets@ub.edu](mailto:xfernandez_busquets@ub.edu)  
doi: 10.1096/fj.10-155507

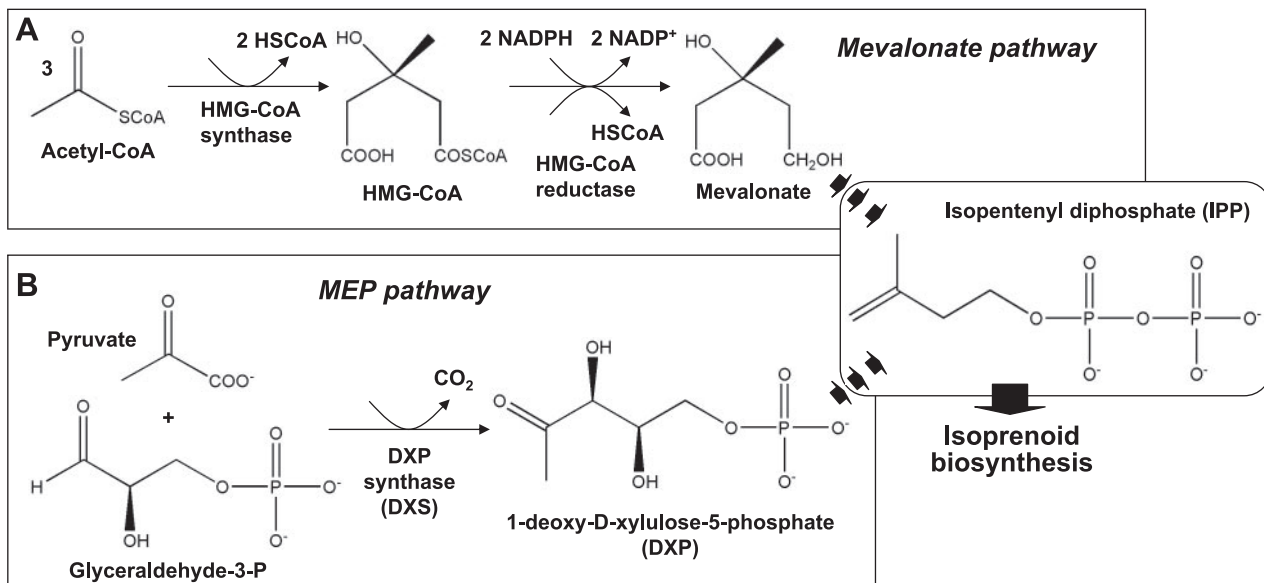


**Figure 1.** Scheme of the first steps of the mevalonate and MEP pathways of isoprenoid biosynthesis. A) Mevalonate pathway. B) MEP pathway.

a single work has attempted to bring into the antimalaria arena the powerful technique of single-molecule handling. During the past decade, single-molecule force spectroscopy (SMFS) has developed into a highly sensitive tool for studying the interaction of individual biomolecules (12, 13). Most SMFS experiments use either optical tweezers or atomic force microscopy to measure dissociation forces of single ligand-receptor complexes in the piconewton range. The binding partners are attached to the nanoscale force sensor and a sample holder, and when both parts are brought into close contact, a specific link between the individual molecules is formed. By increasing the distance between the two surfaces again, the molecular bond is loaded under an external force until it finally breaks, yielding the unbinding force. On systematical variation of the externally applied load while monitoring the mechanistic elasticity of the complex, information can be derived about the kinetic reaction rates, mean lifetime, equilibrium rate of dissociation, dissociation length, and energy landscape of the interaction (14, 15). SMFS experiments have been conceived and applied to measure interactions among single biomolecules (16), including enzyme-substrate (17–21), enzyme-inhibitor (22, 23), receptor-ligand (24–28), antibody-antigen (29–32), protein-DNA (33, 34), redox partners (35), and cell adhesion molecules (36). Furthermore, intramolecular elasticity phenomena, like biopolymer structural transitions (37) and protein unfolding (38), have been investigated by SMFS, giving access to the study of mechanical properties of biomolecules and their related physiological processes (39).

SMFS has been proposed as a method suitable for screening large numbers of ligands (40), an approach that can expedite the discovery of therapeutically useful enzyme inhibitors in a wide affinity range. One of the most attractive characteristics of SMFS is derived from its ability to measure the binding force between individual

enzyme-substrate molecular pairs. As a result, a sought-after inhibitor could theoretically be detected at extremely low concentrations, especially if the inhibitor is irreversible, which is often the most desirable case when searching for drugs with potential pharmacological applications. An SMFS-based sensor might identify potentially useful enzyme inhibitors remaining undiscovered because their concentrations in solution are too low to be detected with conventional methods. Although this theoretical possibility has been hinted insistently, it has never been put to test, and in this field SMFS has gone only as far as being a tool for the characterization of enzyme-substrate interactions. Its real potential for the discovery of new enzyme inhibitors has not been tapped yet, let alone for systems having such small substrates as the 3-carbon molecules G3P and pyruvate.

Here, we have explored the capability of atomic force microscope (AFM) SMFS to identify inhibitors of the DXS catalytic step. The binding forces between the tethered enzyme and either of its two substrates have been characterized at the single-molecule level, and we have studied the sensitivity of this prototype nanosensor for the detection in solution of the DXS inhibitor fluoropyruvate (41). Our data indicate that this proof-of-concept model system can be developed into an efficient screening device for the biodiscovery of new antibiotics and antimalarials.

## MATERIALS AND METHODS

Unless otherwise indicated, analytical-grade reagents were purchased from Sigma-Aldrich (St. Louis, MO, USA). Where the buffer composition is not indicated, the corresponding solutions were made in bidistilled deionized water (Milli-Q system, Millipore, Eschborn, Germany). Where the temperature is not indicated, the corresponding reactions were incubated at room temperature.

## Synthesis of 6-mercaptohexyl glyceraldehyde-3-phosphate derivative

Citations of compounds 1–10 refer to **Fig. 2A**.

### Preparation of 1-(1,3-dioxolan-2-yl)ethane-1,2-diol (compound 2)

Method is from ref. 42. An aqueous solution of  $\text{KMnO}_4$  (32 g, 200 mmol in 300 ml) was added at the rate of  $\sim 20$  ml/min to 2-vinyl-1,3-dioxolane (30 ml, 300 mmol) (compound 1) suspended in 200 ml of water in a 3-necked 1-L flask. The mixture was cooled in an ice bath and vigorously agitated for 2 h with a magnetic stirrer to prevent the overoxidation that results from

the temperature exceeding  $10^\circ\text{C}$ . After  $\text{MnO}_2$  removal by Büchner filtration and evaporation of water, the resulting oil was purified by distillation under reduced pressure (5 mm Hg,  $136\text{--}138^\circ\text{C}$ ) and obtained in a 35% yield (14.0 g).  $^1\text{H-NMR}$  (300 MHz,  $\text{CDCl}_3$ )  $\delta = 4.90$  (d, 1H), 4.00 (m, 4H), 3.93 (m, 1H), 3.74 (d, 2H), 2.90, 3.30 (ss, OH).  $^{13}\text{C-NMR}$  (75 MHz,  $\text{CDCl}_3$ )  $\delta = 103.6, 70.6, 65.8, 65.1, 63.6, 62.5$ .

### Synthesis of 2-tert-butyldimethylsilyloxy-1-(1,3-dioxolan-2-yl)ethane-1-ol (compound 3)

1-(1,3-Dioxolan-2-yl)ethane-1,2-diol (13.4 g, 100 mmol), previously dried by anhydrous  $\text{CH}_3\text{CN}$  coevaporation, was dis-

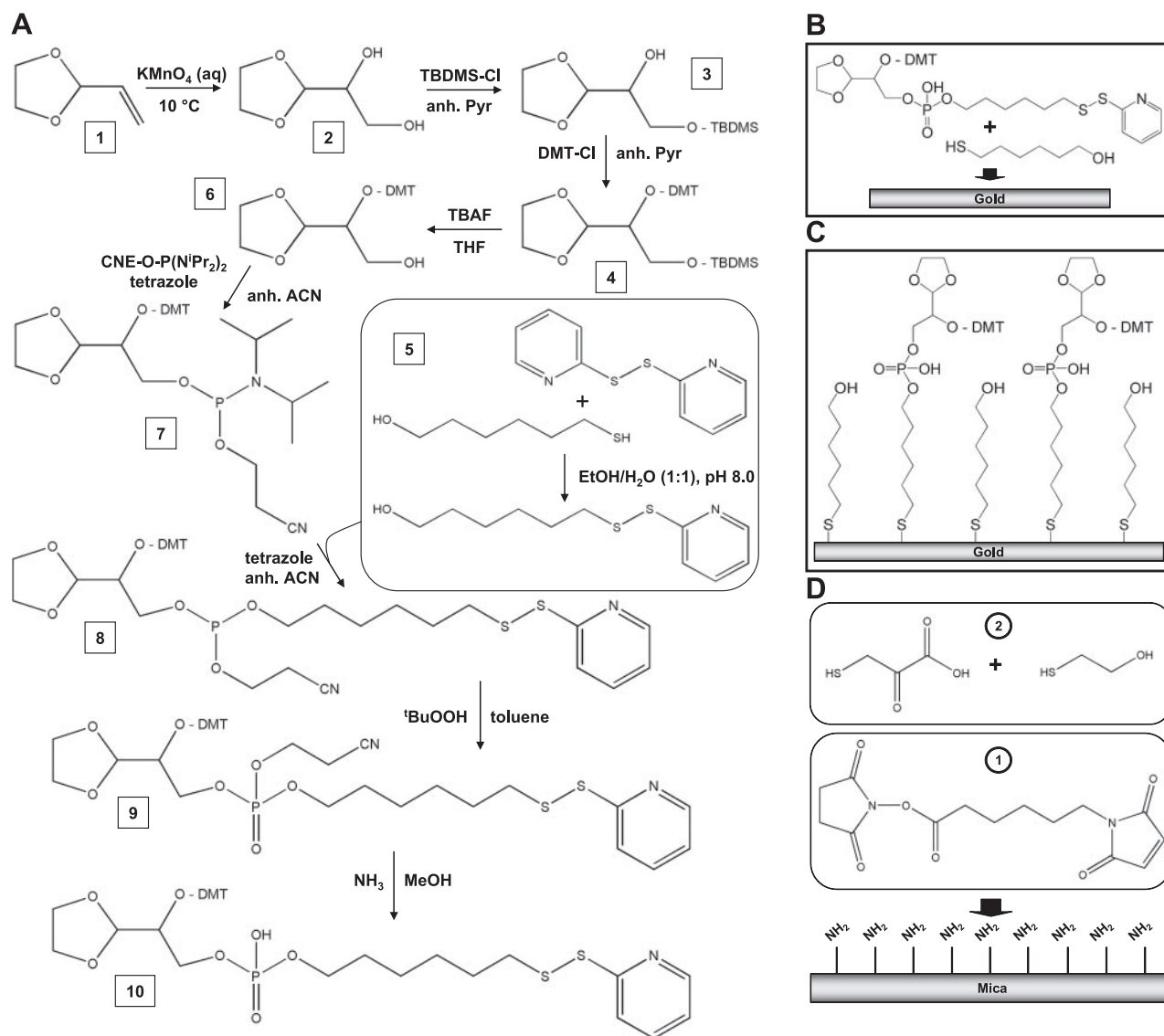


**Figure 2.** Immobilization of G3P and pyruvate. **A**) Scheme of the synthesis of the G3P derivative 6-(pyridin-2-yl)disulfanylhexyl 1-dimethoxytriethoxy-1-(1,3-dioxolan-2-yl)ethane 2-phosphate (compound 10). See Materials and Methods for description of the different synthesis steps (boxed numbers), referred to as compounds 1–10 in the text. **B, C**) Scheme of the process followed for the immobilization of G3P. An equimolar mix of the G3P derivative and mercaptohexanol was deposited on gold-coated mica (**B**). The reaction of thiol groups with gold atoms resulted in the formation of a mixed monolayer of tethered G3P derivative and hydroxyl-terminated chains (**C**). Before starting SMFS assays, the derivative was deprotected to yield tethered G3P. **D**) Scheme of the process followed for the immobilization of pyruvate. APTES-silanized, freshly cleaved mica was treated first with an NHS-PEG-MAL linker to allow for the formation of a bond between the linker NHS groups and the amino groups on the mica surface. The resulting maleimide-functionalized surface was then overlaid with an equimolar mix of mercaptopyruvate and mercaptoethanol to yield a mixed monolayer of tethered pyruvate and hydroxyl-terminated linker.

solved at 1 M in anhydrous pyridine under Ar and kept in an ice bath. TBDMS-Cl (18.1 g, 1.2 eq) was dissolved at 2 M in anhydrous CH<sub>3</sub>CN and slowly added by cannulation to compound 2 under argon. The reaction was monitored by thin-layer chromatography (TLC) analysis and completed in 3 h. After evaporating the solvent, workup by liquid–liquid extraction was performed by 1× citric acid, 2× saturated NaHCO<sub>3</sub>, 1× saturated NaCl against ethyl acetate. After drying the organic phase with MgSO<sub>4</sub>, the solvent was evaporated. TLC and <sup>1</sup>H-RMN analyses showed the presence of a single product, which was obtained in a 65% yield (16.1 g, 65 mmol). <sup>1</sup>H-NMR (300 MHz, CDCl<sub>3</sub>) δ = 4.90 (d, 1H), 3.95–3.82 (m, 3H), 3.69–3.58 (m, 4H), 2.40 (bs, 1H), 0.84 (s, 9H), 0.02 (bs, 6H).

#### Synthesis of 1-dimethoxytrityloxy-1-(1,3-dioxolan-2-yl)ethane-2-ol (compound 6)

Compound 3 (4.5 g, 30 mmol), previously dried by anhydrous CH<sub>3</sub>CN coevaporation, was dissolved at 0.2 M in anhydrous pyridine under an inert atmosphere, and dimethoxytrityl chloride (DMTCl; 12.2 g, 36 mmol, 1.2 eq) was rapidly added. TLC revealed that the reaction was completed after 3 h. After evaporating the solvent, workup by liquid–liquid extraction was performed (1× citric acid, 2× saturated NaHCO<sub>3</sub>, 1× saturated NaCl against ethyl acetate). After drying the organic phase with MgSO<sub>4</sub>, the solvent was evaporated. A crude product (compound 4) was obtained and subjected to the following deprotection step without being purified. Subsequently, the crude was treated for 3 h with tetra(*tert*-butyl)ammonium fluoride hydrate (TBAF, 11.4 g, 36 mmol) dissolved in tetrahydrofuran (THF; 180 ml), and the reaction was monitored by TLC. After solvent evaporation and workup (1× citric acid, 2× saturated NaHCO<sub>3</sub>, 1× saturated NaCl against ethyl acetate), the organic phase was dried with MgSO<sub>4</sub>, and the solvent was evaporated. The resulting products were purified by SiO<sub>2</sub> column chromatography by elution with 60–70% CH<sub>2</sub>Cl<sub>2</sub> in hexane containing 1.5% Et<sub>3</sub>N. The resulting product was obtained in a 72% yield (13.1 g, 22 mmol), and was characterized by <sup>1</sup>H-NMR, <sup>13</sup>C-NMR, and MALDI. <sup>1</sup>H-NMR (300 MHz, CDCl<sub>3</sub>) δ = 7.56–7.24 (m, 9H), 6.82 (d, 4H), 4.9 (d, 1H), 3.91 (m, 4H), 3.76 (m, 1H), 3.64 (d, 2H), 2.78 (s, -OH). MALDI-EM (trihydroxyacetophenone matrix, positive mode) *m/z*: 453.75 [M+Na]<sup>+</sup>, 474.78 [M+K]<sup>+</sup>. <sup>13</sup>C-NMR (75 MHz, CDCl<sub>3</sub>) δ = 169.4, 158.6, 154.8, 145.3, 144.1, 135.2, 135.1, 128.3, 128.8, 127.2, 126.7, 126.6, 112.8, 102.0, 72.0, 63.8, 60.1, 54.2, 54.1.

#### Synthesis of 6-(pyridin-2-ylidisulfanyl)hexane-1-ol (compound 5)

Method is from ref. 43. Dithiodipyridine (5.5 g, 25 mmol) was dissolved at 0.1 M in ethanol/water (1:1) at pH 8.0, and it was added to a 0.1 M solution of 6-mercaptohexanol in ethanol (1.7 g, 12.5 mmol in 125 ml). After stirring for ~1.5 h, the solvent was evaporated and redissolved in ethyl acetate, and the resulting organic phase was washed with water to neutrality. The organic phase was dried with MgSO<sub>4</sub>, and after evaporating the solvent, purification was performed by SiO<sub>2</sub> column chromatography, eluting with a gradient from 0 to 1.5% methanol in CH<sub>2</sub>Cl<sub>2</sub>. The product was obtained as a clear oil in a 62% yield (1.9 g, 7.8 mmol). According to NMR analyses, no further purification was required. <sup>1</sup>H-NMR (300 MHz, CDCl<sub>3</sub>) δ = 8.44 (d, 1H), 7.70 (m, 1H), 7.63 (m, 1H), 7.08 (dd, 1H), 3.62 (t, 2H), 2.79 (t, 2H), 1.71 (m, 2H), 1.53 (m, 4H), 1.36 (m, 2H).

#### Synthesis of 6-(pyridin-2-ylidisulfanyl)hexyl 1-dimethoxytrityloxy-1-(1,3-dioxolan-2-yl)ethane 2-phosphate (compound 10)

Alcohol (compound 6; 800 mg, 1.9 mmol) was coevaporated with anhydrous acetonitrile, further dried in high vacuum for 60 min, and finally dissolved in anhydrous acetonitrile at 0.1 M under an inert atmosphere. *O*-cyanoethyl-*N,N,N,N*-tetra-isopropylphosphordiamidite (690 mg, 2.28 mmol, 1.2 eq) was added, followed by tetrazole (66 mg, 1.0 mmol, 0.5 eq), with continuous stirring and under extreme dry and inert conditions. The reaction was followed by TLC (ethyl acetate/CH<sub>2</sub>Cl<sub>2</sub>/triethylamine, 45:45:10), and it was completed in 3 h. After removing the solvent by evaporation, the crude product was redissolved in ethyl acetate, washed with aqueous 10% NaHCO<sub>3</sub> and brine, and dried with Na<sub>2</sub>SO<sub>4</sub>. Analyses by <sup>1</sup>H-NMR and <sup>31</sup>P NMR showed a mixture of phosphoramidite isomers, which did not need further purification to carry out the following reaction. <sup>1</sup>H-NMR (400 MHz, CDCl<sub>3</sub>) δ = 7.60–7.10 (m, 9H), 6.82 (d, 4H), 3.82 (d, 1H), 4.20–3.80 (m, 3H), 3.78 (s, 6H), 3.78–3.20 (m, 6H), 2.72–2.42 (m, 2H), 1.40–1.00 (m, 12H). <sup>31</sup>P-NMR (81 MHz, CDCl<sub>3</sub>) δ = 148.4, 147.8.

The crude phosphoramidite (500 mg, 0.61 mmol) was dissolved in anhydrous acetonitrile (1 ml) and compound 5 (146 mg, 0.6 mmol), and tetrazole (42 mg, 0.6 mmol) was added. According to TLC analysis (ethyl acetate/CH<sub>2</sub>Cl<sub>2</sub>/triethylamine, 45:45:10), the coupling (compound 8) was completed in 5 h. The mixture was then treated with 0.5 ml of 6 M <sup>t</sup>BuOOH/toluene to produce oxidation of phosphite to phosphate, to obtain compound 9. The solvent was evaporated, and the resulting crude product was dissolved in 20 ml of 7 N NH<sub>3</sub> in methanol to produce the cyanoethyl group removal and the obtainment of compound 10. The solvent was again evaporated, and the crude product was purified first by precipitation in cold hexane and subsequently by SiO<sub>2</sub> column chromatography (gradient from 0.2 to 20% methanol in CH<sub>2</sub>Cl<sub>2</sub>). Product was obtained as a clear oil in a 14% yield, and it was characterized by <sup>1</sup>H-NMR, <sup>31</sup>P-NMR, and electrospray mass spectrometry. <sup>1</sup>H-NMR (400 MHz, CDCl<sub>3</sub>) δ = 8.47 (d, 1H), 7.71 (d, 1H), 7.62 (t, 1H), 7.51 (d, 2H), 7.39 (d, 4H), 7.25–7.18 (m, 3H), 7.06 (dd, 1H), 6.80 (d, 4H), 5.49 (m, 1H), 3.88–3.77 (m, 3H), 3.63 (t, 2H), 3.48 (s, 6H), 3.47–3.20 (m, 4H), 2.80 (t, 2H), 1.72–1.30 (m, 10H). <sup>31</sup>P-NMR (81 MHz, CDCl<sub>3</sub>) δ = 0.60. ESI-MS (negative mode) *m/z* 740.5 [M-H]<sup>-</sup>, 740.5 [M+Na-2H]<sup>-</sup>.

#### Construction of the *Escherichia coli* DXS expression vector pET-23-DXS

The coding region of *E. coli* DXS (64 kDa), cloned into the expression vector pT7-7 (44), was amplified by PCR using *Pfu* DNA polymerase and primers T7 (5'-TAATACGACTCAC-TATAGG-3') and pET-23-*XhoI* (5'-CGCTCGAGTCCTGCCAG-CCAGGCCTTGATTTTGGC-3'). After digestion with *NdeI* and *XhoI*, the amplified DNA fragment was ligated into the same sites of the expression vector pET-23b. Strain DH5α (Promega, Madison, WI, USA) was used as the recipient during this transformation. Positive clones were identified by DNA sequencing using Big Dye Terminator v3.1 cycle sequencing kit (Applied Biosystems, Foster City, CA, USA). The resulting plasmid was designated pET-23-DXS, which produces the C-terminal histidine-tagged protein.

#### Overexpression and purification of *E. coli* DXS

BL21 (DE3) pLysS cells carrying pET-23-DXS were grown in Luria-Bertani medium supplemented with 100 μg/ml ampi-

collin and 34  $\mu\text{g}/\text{ml}$  chloramphenicol at 22°C to an  $\text{OD}_{600}$  of 0.3–0.4 and then induced with 0.3 mM isopropyl  $\beta$ -D-thiogalactoside for 18–20 h. Bacterial cells were recovered by centrifugation, and the cell pellet was resuspended in 40 mM Tris-HCl buffer, pH 8.5, containing 100 mM NaCl, 10 mM imidazole, 1 mM  $\text{MgCl}_2$ , 5 mM  $\beta$ -mercaptoethanol, 1 mM TPP, 1 mg/ml lysozyme, 1 mM Pefabloc SC Plus (Roche, Basel, Switzerland), and one tablet of complete EDTA-free protease inhibitor cocktail (Roche). After incubation at 4°C for 30 min the lysate was sonicated during 20 s and centrifuged at 12,000  $g$  for 45 min at 4°C. Recombinant DXS was purified by  $\text{Ni}^{2+}$  affinity chromatography (1 ml Hi-Trap chelating column, GE Healthcare, Little Chalfont, UK) with a linear gradient from 10 to 500 mM imidazole. Fractions containing DXS were pooled; dialyzed against a buffer containing 50 mM Tris-HCl (pH 7.5), 137 mM NaCl, 1% Tween 20, and 1% Triton X-100; snap-frozen in liquid  $\text{N}_2$ ; and finally stored at  $-80^\circ\text{C}$  until use. Protein concentration was determined by the method of Bradford (45), using bovine serum albumin as standard.

### Immobilization of molecules for SMFS

#### Pyruvate

Freshly cleaved muscovite mica slides (Metafix, Montdidier, France) were gas phase silanized with (3-aminopropyl)triethoxysilane (APTES) in a vacuum desiccator according to established protocols (46), and overlaid with 1 mM *N*-succinimidyl-6-maleimido caproate overnight. The resulting maleimide groups were used to bind the thiol groups in mercaptopyruvate and mercaptoethanol (added as a 1 mM equimolar mix) to yield a layer of immobilized pyruvate. Surface-bound mercaptoethanol provided a hydrophilic environment in the bidimensional molecular film.

#### G3P

An equimolar mix of compound 10 and mercaptohexanol (1 mM each in 100% EtOH) was directly deposited overnight onto gold-coated mica surfaces prepared with the template-stripped gold method (47). The reaction between the SH group generated on the G3P derivative and Au atoms formed a layer of immobilized G3P after treatment with 50%  $\text{CH}_3\text{COOH}$  for 30 min to remove protecting DMT and ketal groups. Mercaptohexanol bound to the surface through its thiol group provided a hydrophilic environment in the bidimensional molecular film.

#### DXS

APTES-silanized silicon nitride tips (Olympus Corp., Tokyo, Japan) were first modified with a combination of bifunctional linkers. Tips were immersed overnight in a 1 mM solution of *N*-hydroxysuccinimide-polyethyleneglycol-maleimide (NHS-PEG-MAL) 3400 linker (polydispersity index <1.05; Nektar, Huntsville, AL, USA), rinsed, and then treated with a 1 mM 11-mercaptoundecanoic acid solution in EtOH. The carboxyl-functionalized tips were then activated using NHS and *N*-ethyl-*N'*-(3-diethylaminopropyl)carbodiimide (EDC) coupling (48). The resulting NHS group reacted with the amino groups from the side chains of Lys residues in DXS, which was added in SMFS assay buffer (see below) at a concentration of 70  $\mu\text{g}/\text{ml}$ . After 1 h, unreacted ester groups were finally capped with a brief immersion in 1 M ethanolamine-HCl, pH 8.0.

### AFM imaging

Tapping-mode AFM images were taken in 2.5 mM  $\text{MgCl}_2$ , 1 mM TPP, and 40 mM Tris-HCl (pH 8) with a Molecular Force Probe 3D microscope (Asylum Research, Santa Barbara, CA, USA). Silicon nitride tips mounted on pyramidal 200- $\mu\text{m}$  cantilevers ( $k = 0.02 \text{ N/m}$ ) were purchased from Olympus. Frequency was set to 5–10% lower than resonance, with a free amplitude of 1 V and a set point kept below 20% of free amplitude.

### Immobilization of DXS on synthetic beads

DXS (2.5 mg/ml), dissolved in 140 mM NaCl, 1% Tween 20, 1% Triton X-100, and 50 mM Tris-HCl (pH 7.5), was passed through a protein desalting column equilibrated with 100 mM MOPS (pH 6.4), and finally immobilized onto synthetic beads containing a NHS ester at the end of a 10C spacer arm (AffiGel 10; Bio-Rad, Hercules, CA, USA). Desalted enzyme (2.25 ml) was added to 100  $\mu\text{l}$  of beads prewashed with 10 mM sodium acetate (pH 4.5), and after 1 h incubation, the mix was centrifuged, and the supernatant was removed. Unreacted sites were blocked by treatment for 1 h with 1 M ethanolamine-HCl, pH 8.0. Pelleted beads (40  $\mu\text{l}$ ) were used for enzyme activity assays.

### Time-of-flight secondary ion mass spectroscopy (TOF-SIMS) characterization of immobilized pyruvate and G3P

Positive polydimethylsiloxane stamps (5- $\mu\text{m}$ -diameter cylindrical posts) were immersed for 5 min in 1 mM solutions of mercaptopyruvate or compound 10. Stamps with the adsorbed molecules were then dried under  $\text{N}_2$  flow and microcontact printed on mica and gold surfaces functionalized as described above for SMFS assays. TOF-SIMS analyses were performed using a TOF-SIMS IV (ION-TOF GmbH, Münster, Germany) operated at a pressure of  $5 \times 10^{-9}$  mbar. Samples were bombarded with a pulsed bismuth liquid metal ion source ( $\text{Bi}^{3+}$ ), at an energy of 25 keV. The gun was operated with a 20-ns pulse width, 0.3-pA pulsed ion current for a dosage lower than  $5 \times 10^{11}$  ions/ $\text{cm}^2$ , well below the threshold level of  $1 \times 10^{13}$  ions/ $\text{cm}^2$  generally accepted for static SIMS conditions. Secondary ions were detected with a reflectron TOF analyzer, a multichannel plate, and a time-to-digital converter (TDC). Measurements were performed with a typical acquisition time of 20 s, at a TDC time resolution of 200 ps. Charge neutralization was achieved with a low-energy (20-eV) electron flood gun. Secondary ion spectra and images in both positive and negative mode were acquired from randomly rastered surface areas of  $500 \times 500 \mu\text{m}$  along the microslide. Secondary ions were extracted with 2 kV voltage and postaccelerated to 10 keV kinetic energy just before hitting the detector. The maximum mass resolution,  $r = m/D_m$ , was  $\sim 9000$ , where  $m$  is the target ion mass and  $D_m$  is the resolved mass difference at the peak half-width.

### Surface plasmon resonance (SPR)

SPR assays were done in a TI100 SPR instrument (Biacore, GE Healthcare) using CM5 sensor chips for the immobilization of pyruvate and G3P through thiol groups. NHS, EDC, and 2-(2-pyridinyldisulfanyl)ethaneamine (PDEA) were also obtained from Biacore. Equal volumes of 50 mM NHS and 200 mM EDC were mixed together, and 20  $\mu\text{l}$  of the resulting solution were injected at 10  $\mu\text{l}/\text{min}$  into the flow cell of the sensor chip. For the immobilization of pyruvate, 40  $\mu\text{l}$  of 80 mM PDEA was injected, followed by 50  $\mu\text{l}$  of 50 mM mercaptopyruvate, and finally by 40  $\mu\text{l}$  of 50 mM 2-mercaptoethanol

to cap unreacted activated sites. For the immobilization of G3P, 40  $\mu$ l of 40 mM cystamine (pH 8.5) was injected, followed by 40  $\mu$ l of 0.1 M dithioerythritol, and finally by 50  $\mu$ l of a 50 mM solution in 70% EtOH of the G3P derivative compound 10. The remaining unreacted sites were finally capped with 40  $\mu$ l of 1 M NaCl and 20 mM PDEA, pH 4.0. DMT and ketal-protecting groups were removed with 40  $\mu$ l of a 100 mM HCl, 1 M NaCl solution, also used to regenerate the chip surfaces by flushing it for 30 s at a flow rate of 30  $\mu$ l/min. For the control flow cell, the NHS/EDC-activated chip surfaces were flushed with 40  $\mu$ l of an 80 mM ethanolamine-HCl solution to cap all the reacting sites.

SPR assays were performed at 20°C in running buffer (150 mM NaCl, 2.5 mM MgCl<sub>2</sub>, and 10 mM HEPES, pH 7.4). Enzyme solutions in running buffer containing 1 mM TPP were injected at 15  $\mu$ l/min during 100 s, with DXS alone or in the presence of different concentrations of pyruvate, fluoropyruvate, or G3P. Data were recorded from 30 s before injection start to 200 s after the end of injection. Biacore T100 1.1 evaluation software was used for analysis, which enabled a double blank subtraction from two control samples: enzyme-containing solution flushed through the control cell and buffer without enzyme flushed through immobilized pyruvate- and G3P-containing cells. Rate and equilibrium constants were obtained by analyzing the kinetics of binding with the analysis software for biosensor data Scrubber2 (BioLogic Software Pty. Ltd., Campbell, Australia).

### DXS activity determination

DXS enzymatic activity was usually determined by a spectrophotometric assay using purified 1-deoxy-D-xylulose 5-phosphate reductoisomerase (DXR) as coupled enzyme (49). Recombinant *E. coli* DXR was obtained as described elsewhere (50). All kinetic measurements were made at 37°C in triplicate. The standard reaction mixtures were done in 100 mM Tris-HCl buffer (pH 7.8) containing 1 mM TPP, 1 mM MgCl<sub>2</sub>, 1 mM MnCl<sub>2</sub>, 1 mM DTT, 0.15 mM NADPH, 1 mM pyruvate, 1  $\mu$ g DXS, and 6  $\mu$ g DXR in a final volume of 0.2 ml. The reaction was initiated by adding 1 mM DL-glyceraldehyde 3-phosphate. Initial reaction velocities were determined following the oxidation of NADPH by monitoring A<sub>340</sub> in a Benchmark Plus spectrophotometer (Bio-Rad). One enzyme unit is defined as the amount of DXS catalyzing the transformation of 1  $\mu$ mol of pyruvate and D-glyceraldehyde 3-phosphate into DXP under the conditions of the assay. As an alternative method for DXS activity analysis, we used TLC on 60 F254 Silicagel plates (Merck, Wilmington, DE, USA) [MeOH/H<sub>2</sub>O/25% (v/v) NH<sub>3</sub>/CH<sub>3</sub>COOH, 50:25:7.5:1], stained with  $\rho$ -anisaldehyde/sulfuric acid/acetic acid (2.4%:3.6%:1.2%, v/v) (51).

### Force spectroscopy measurements

Force spectroscopy studies were performed in a Molecular Force Probe 3D microscope (Asylum Research, Santa Barbara, CA, USA). Silicon nitride tips mounted on triangular 200- $\mu$ m cantilevers ( $k = 0.02$  N/m) were purchased from Olympus. The spring constant of every tip was individually measured through the equipartition theorem using the thermal noise of the cantilever (52). SMFS assays were performed in 2.5 mM MgCl<sub>2</sub>, 1 mM TPP, 40 mM Tris-HCl, pH 8. The configurations used consisted of DXS on the cantilever, pyruvate or G3P on mica or gold surfaces, respectively, and the buffer alone or buffer containing substrates or fluoropyruvate. The cantilever was lowered to the surface manually, and the AFM was operated such that it moved away from and then toward the sample surface during the course of each

cycle. The pressure applied at the contact point was <1 nN. Based on preliminary assays performed at different loading rates, the SMFS data presented were obtained with a pulling velocity of 0.5  $\mu$ m/s, except where otherwise indicated. The same tip and surface were used with the different substrate and inhibitor solutions of a single experiment. For each configuration, 1500 force plots were recorded and taken at different points on the functionalized surfaces. Data analysis and statistical treatments were done with the software provided by the AFM manufacturer (IgorPro 5.0.4.8; WaveMetrics Inc., Lake Oswego, OR, USA). To restrict the analysis to single-molecule interactions, peak selection was generally done manually, setting a maximum length threshold of 100 nm (which corresponds to the maximum length of the PEG linker), considering only the last adhesion event of force-extension curves. Force curves with peaks above 1 nN were likely arising from non-specific adhesions, and we did not consider them as enzyme-substrate interactions, although they were included in the statistics calculations as curves without specific binding event.

## RESULTS

The planned configuration of SMFS assays consisted of DXS-functionalized AFM cantilevers and pyruvate- or G3P-functionalized surfaces *via* heterobifunctional linkers (32). Such strategy introduces a distance between interacting molecules and surfaces, adds steric flexibility for the binding partners, and guarantees an almost complete reduction of unspecific binding events (53), although it might affect the calculation of the apparent kinetic and thermodynamic enzymatic parameters (23). Because *E. coli* DXS has 36 lysines, of which only K289 is present in the active center (54), we followed established protocols (48) for the covalent linkage of the enzyme to SiN<sub>3</sub> cantilevers through the lateral amino group in lysine residues, using a monodisperse  $\sim$ 100 nm-long polyethylene glycol (PEG) linker (Fig. 3). As shown below, DXS immobilized in this way was active in binding its two substrates, pyruvate and G3P. The immobilization of G3P was done through its phosphate based on data reporting that this group is exposed to the solvent and does not participate in the enzymatic reaction (54). Thus, a G3P derivative containing a gold-reacting linker was synthesized (Fig. 2A) and deposited onto gold-coated mica surfaces to obtain self-assembled monolayers (SAMs) of the G3P derivative following reduction of disulfide groups by gold (Fig. 2B, C). To obtain pyruvate SAMs, (3-aminopropyl)triethoxysilane-silanized flat mica surfaces were functionalized with mercaptopyruvate through a maleimido-PEG-N-hydroxysuccinimide linker (Fig. 2D). The choice of the thiol group located in the C3 atom of mercaptopyruvate for the immobilization of the substrate was made on the basis of data showing that this carbon is not implicated either in the initial formation of the adduct with TPP or in the forthcoming steps of the reaction mechanism (4, 54). Additional experimental evidence validating our strategy indicated that DXS was active in metabolizing hydroxypyruvate instead of pyruvate (55), which sug-

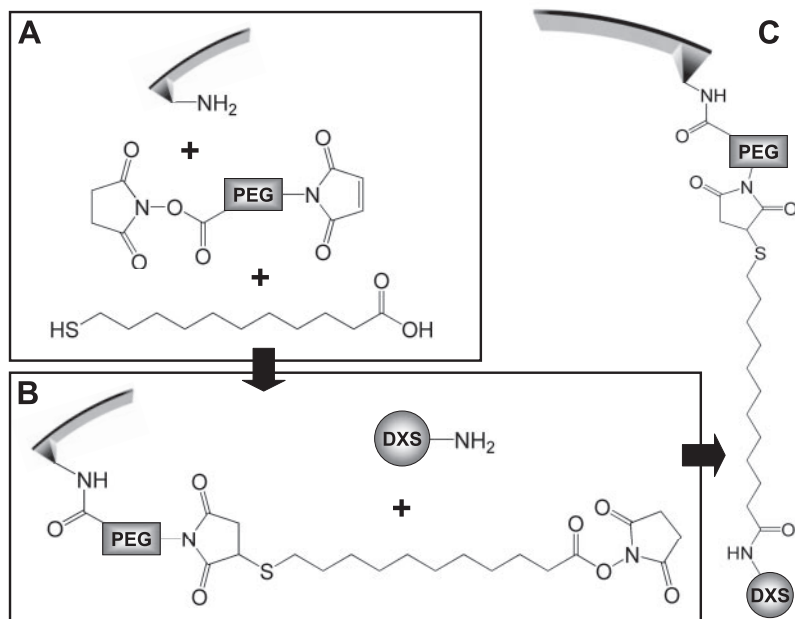


**Figure 3.** Immobilization of DXS on AFM cantilevers. *A)* Treatment of silanized AFM cantilevers with NHS-PEG-MAL and 11-mercaptopropionic acid linkers to generate a carboxyl-terminated tether. *B)* Activation of the carboxyl group with EDC/NHS to make it reactive with amino lateral groups in DXS. *C)* Scheme of DXS immobilization on AFM cantilevers.

gests that an additional group in C3 did not affect the enzyme-substrate interaction.

TOF-SIMS (56) was used to characterize the correct immobilization of pyruvate and G3P on mica and gold surfaces, respectively (Fig. 4). A fragment of 74.97 Da was consistent with the presence of pyruvate after the crosslinking procedure onto mica (Fig. 4A). Other molecules detected were a sulfur-containing derivative (60.96 Da) and a part of the bifunctional linker (198.85 Da). Measures of G3P patterns on gold detected the presence of phosphates (97.29 Da), thiopyridine (110.35 Da), and different species originated from the synthesized G3P derivative (at 623.70, 632.20, and 765.06 Da) (Fig. 4B).

Bidimensional on-the-surface dilution of pyruvate and (after deprotection of the derivative) G3P in a hydrophilic environment was achieved by introduction of hydroxyl-terminated linkers to form mixed SAMs that reduced sterical hindrances between the interacting molecules in SMFS experiments (Fig. 5A, B). AFM imaging of surfaces, functionalized with pyruvate, G3P, or DXS following the chemistry described above, showed the deposition of homogeneous monolayers (Fig. 5C–E), with root mean square roughness of 0.7, 1.1, and 1.3 nm, respectively. Binding between DXS and its substrates crosslinked to surfaces was first explored by surface plasmon resonance (SPR). Mercaptopyruvate and the G3P derivative were bound to SPR chips with the same chemistry used later in SMFS assays, to yield immobilized pyruvate and G3P. DXS in solution binds efficiently to both tethered substrates in a concentration-dependent process (Fig. 5F, G). Complete dissociation was not achieved in either case, in agreement with the existence of a strong interaction between DXS and its two covalently immobilized substrates. Different substrate concentrations were assayed, which provided optimal pyruvate and G3P densities of 65 and 780 response units, respectively. Higher densi-

ties resulted in reduced DXS binding, probably because of steric hindrance due to densely packed substrate layers. The integrated rate equations were fitted to the association and dissociation sensorgrams (57), obtaining both on- and off-rate constants, and thus the equilibrium dissociation constants,  $K_{D,pyruvate} = \sim 57 \mu\text{M}$  and  $K_{D,G3P} = \sim 81 \mu\text{M}$ , whose values did not differ significantly from those derived from enzyme assays in solution (100 and 440  $\mu\text{M}$ , respectively) (58).

The measured rupture force of the interaction between DXS tethered to AFM cantilevers and surface-bound pyruvate was found to be between 150 and 250 pN, depending on the loading rate (Figs. 5H and 10B). To estimate the time and number of approach/retract curves during which the enzyme maintained its activity, we routinely performed controls where the binding probability for a given system configuration was checked throughout control experiments. The binding probability (%) was calculated as the number of force curves with  $\geq 1$  specific enzyme-substrate adhesion event *vs.* the total number of curves. The data obtained indicated that DXS bound its immobilized substrates without decrease in rupture force or binding probability for a time between 6 and 8 h, or 6000 recorded curves. Specific adhesion events were indicated by analysis of the force curves immediately before the jump-off contact. Specific interactions are characterized by a typical worm-like chain slope in the adhesion zone of the retracting plot just before rupture (Fig. 5H) (12, 22). Such an analysis is greatly facilitated by the use of suitable flexible linkers connecting the inorganic surfaces with the biomolecules. In addition, we considered only ruptures that took place at a distance from the surface  $< 100$  nm, which corresponds approximately to the linker length. Examples of multiple-peak curves and of unspecific tip-surface binding are provided in Fig. 6. Finally, force peaks above 1 nN were not considered because they were relatively few and far off the gaussian median

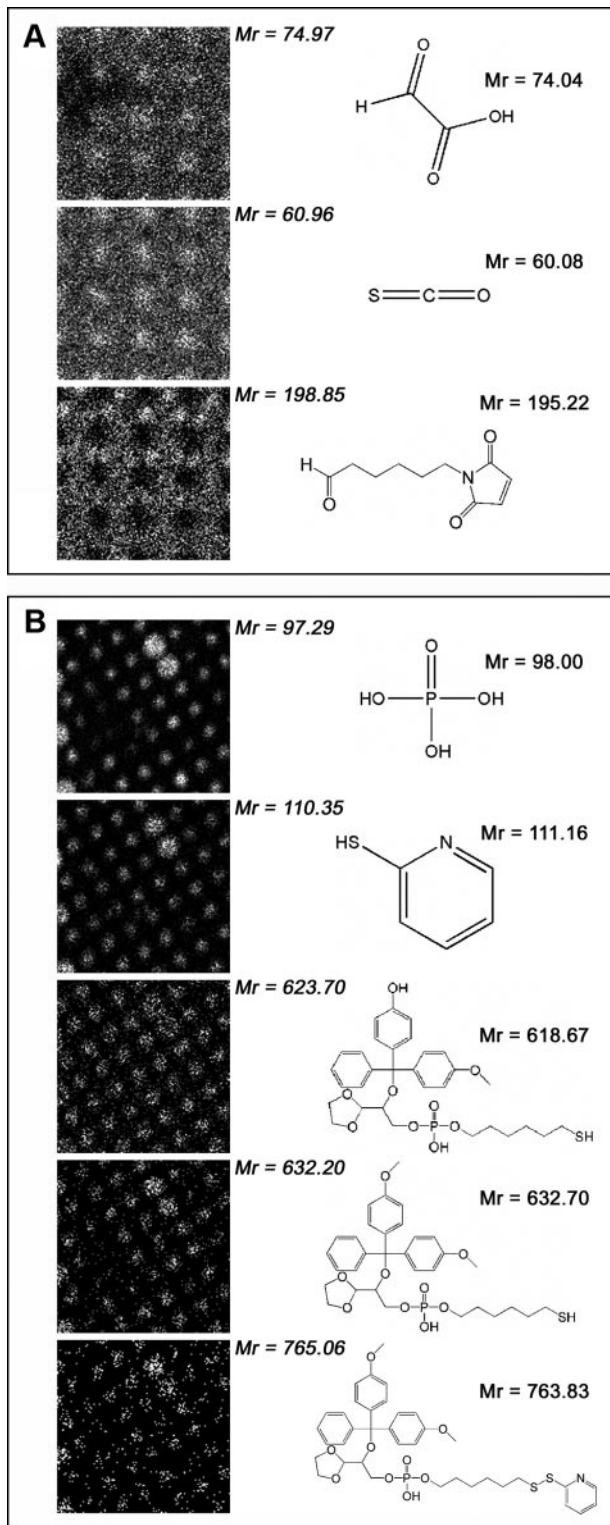


**Figure 4.** TOF-SIMS analysis of tethered pyruvate immobilized on mica (A) and of tethered G3P immobilized on gold (B).

centered at  $\sim 200$  pN in control experiments. Other controls involved testing the DXS-free PEG linker on substrate-functionalized surfaces. In such assays, the force distributions obtained lacked the 200 pN maximum and presented instead a few events distributed below and above this value (Fig. 7), resulting from

unspecific linker-surface interactions. Because of the large difference in molecular mass between the PEG linker and DXS (3.4 and 64.0 kDa, respectively), the unspecific adhesion events experienced by the PEG linker alone will be reduced  $\sim 20$ -fold in the presence of DXS. Force plots in competition SMFS assays indicated that maximal adhesion probability between DXS and G3P was obtained on addition of soluble pyruvate (Fig. 8A), yielding rupture forces similar to those for the DXS-pyruvate association. These data are consistent with SPR results showing that the presence of soluble pyruvate increased the interaction of DXS with a G3P-functionalized surface (Fig. 8B). The presence of TPP in solution was necessary in SPR assays for the detection of binding between DXS and G3P (Fig. 8B) or pyruvate (Fig. 8C), whereas in SMFS experiments, the interaction of the enzyme with either substrate was not dependent on the presence of the cofactor.

Competition SMFS assays in the presence of 1 mM pyruvate showed that soluble G3P interfered with the adhesion of DXS to immobilized G3P in a concentration-dependent process (Fig. 8D), with a significant inhibitory effect at 0.1 mM G3P. In contrast, 1 mM soluble pyruvate had to be present to decrease the probability of DXS binding to immobilized pyruvate (Fig. 8E). In this case, the addition of soluble G3P did not increase the binding probability between DXS and pyruvate (data not shown). As a routine control performed at the end of each SMFS assay, force peaks were recovered on removal of the soluble competitor, confirming DXS performance and validating the data obtained. More complex force distributions were often obtained in some SMFS experiments (Fig. 8D, E, G), usually in the form of adhesion peaks at  $\sim 400$ , 600, and 800 pN, which might represent simultaneous multiple binding events. In agreement with SMFS data, SPR competition assays for the binding of DXS between immobilized pyruvate and soluble pyruvate or the enzyme inhibitor fluoropyruvate at high concentrations showed that the presence of soluble ligands decreased the affinity of the enzyme for the homologous surface-bound substrate (Fig. 8C). SMFS binding competition assays in the presence of soluble fluoropyruvate at lower concentrations showed that the DXS inhibitor was significantly more efficient than soluble pyruvate in blocking the interaction with immobilized pyruvate. The presence of 0.1 mM fluoropyruvate (Fig. 8F) reduced to 2% the binding probability between the enzyme and surface-bound pyruvate, whereas 1 mM fluoropyruvate was necessary to inhibit DXS binding to G3P (Fig. 8G). Sensitivity could be improved by reducing the amount of immobilized DXS on the AFM cantilever. For the configuration DXS-pyruvate, using 100 times less enzyme resulted in a 10-fold sensitivity increase, with 10  $\mu$ M fluoropyruvate reducing by  $>85\%$  the DXS-pyruvate interaction (Fig. 9A).

Although the covalent immobilization of DXS did not abolish the binding to its substrates, we had no information on how this affected the metabolic competence of the enzyme. To explore this issue we per-

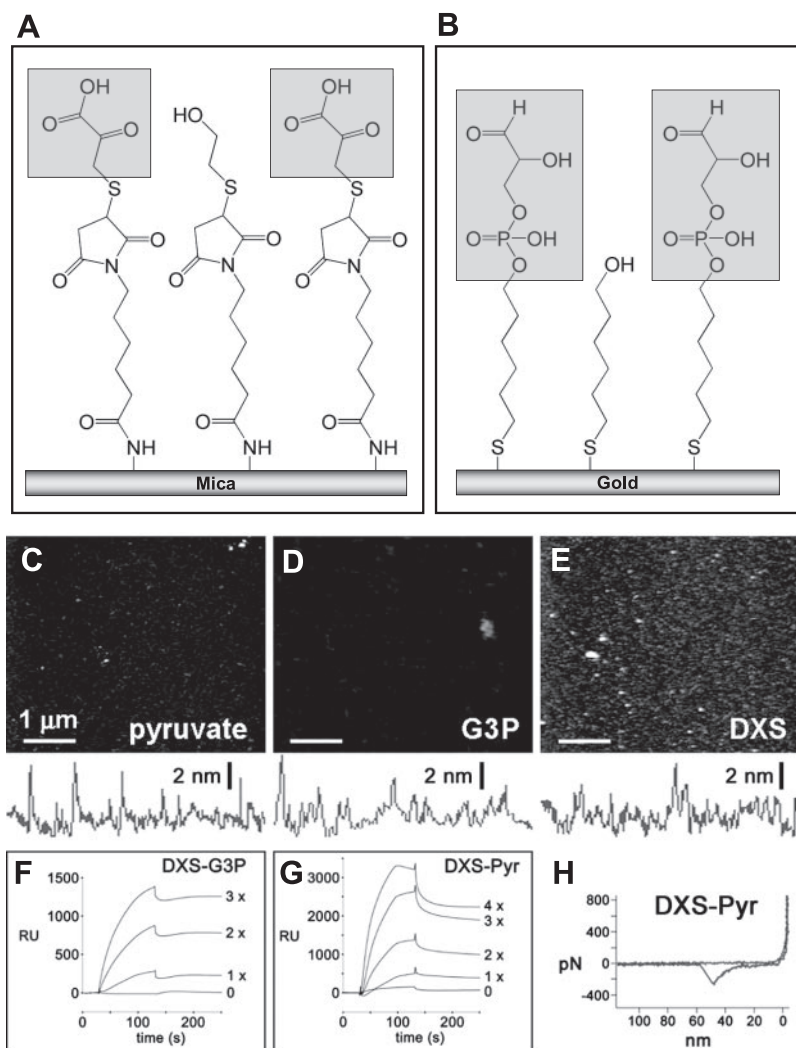


**Figure 5.** DXS binding to covalently immobilized pyruvate and G3P. *A*) Scheme of mica surfaces functionalized with pyruvate (boxed and shaded). *B*) Scheme of gold surfaces functionalized with G3P (boxed and shaded). *C–E*) AFM images of pyruvate-coated mica (*C*), G3P-coated gold (*D*), and DXS immobilized on mica with the same chemistry used for its binding to cantilevers (*E*). Vertical *z* scale is 20 nm. Representative cross-section analysis of surface roughness is presented at bottom of each image. *F*, *G*) SPR assays of DXS binding to its immobilized substrates. *F*) G3P binding analysis:  $1\times \sim 37 \mu\text{g/ml}$ . *G*) Pyruvate binding analysis:  $1\times \sim 46 \mu\text{g/ml}$ . All samples contained 1 mM TPP. *H*) Typical approach-retract SMFS force cycle for a single DXS-pyruvate binding event.

formed enzyme activity assays with DXS crosslinked to *N*-hydroxysuccinimide-functionalized agarose beads with the same chemistry as that used for SMFS experiments. Thin-layer chromatography analysis of the reaction products revealed the presence of DXP (**Fig. 10A**), indicating that tethered DXS could metabolize its substrates, although a quantitative estimation showed that the immobilized enzyme retained only  $\sim 14\%$  of its catalytic activity in solution.

Pulling experiments in which the tip-surface separation speed is changed in such a way that the force per unit time (loading rate) acting on the molecular bond under study is changed over orders of magnitude are referred to as dynamic force spectroscopy (DFS). DFS permits a deeper analysis of the mechanics of single-molecule assays, providing information on dissociation constants and the average lifetimes of molecular interactions. According to the standard model of thermally driven dissociation under external force (14), the measured dissociation forces ( $F_{\text{max}}$ ) depend on the experimental retraction velocity and should be represented against the corresponding loading rates in a DFS plot. To obtain molecular loading rates, the retraction velocity is multiplied by the elasticity of the system, which is determined by fitting the slope of every single force

curve just before dissociation. Generally, the measured  $F_{\text{max}}$  obeys the following law (Eq. 1):

$$F_{\text{max}} = \frac{k_B T}{x_B} \ln \frac{x_B r}{k_B T k_{\text{off}}} \quad (1)$$

where  $k_B T$  and  $r$  denote thermal energy and the loading rate, respectively.  $x_B$  is a length parameter along the reaction coordinate representing the distance between the minimum of the binding potential and the transition state separating bound and free states, which is commonly referred to as the reaction length.  $k_{\text{off}}$  is the thermal off-rate constant under zero external load and can be deduced by linearly extrapolating the experimental data in the DFS plot to zero external force ( $F=0$ ). The inverse relation of  $k_{\text{off}}$  to the average lifetime of the complex,  $\tau$  ( $k_{\text{off}} = \tau^{-1}$ ), allows a direct way of evaluating its stability. For the interaction DXS-pyruvate, when we applied mechanical force in a range of loading rates, the logarithmic DFS plot of the measured SMFS data shows the presence of two force regimes according to Eq. 1 (Fig. 10B). For the single-molecule process, quantitative analysis at low and high loading rates yields, respectively, dissociation constants of  $k_{\text{off}} = 6.1 \times 10^{-4} \pm 7.5 \times 10^{-3}$  and  $1.3 \times$

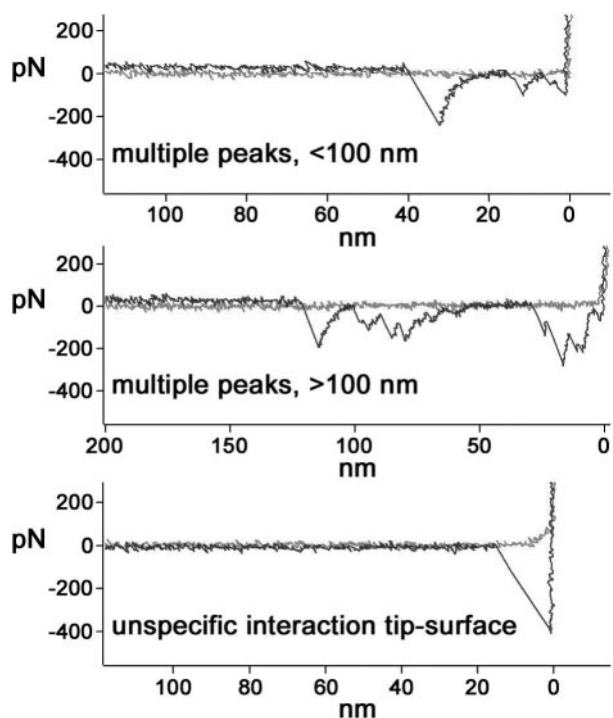


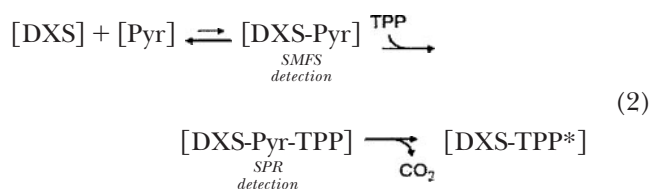
**Figure 6.** Examples of SMFS force-extension graphs for the DXS-pyruvate binding analysis. Top graph corresponds to a pull with multiple interactions where the last peak on the left was considered to be a specific adhesion event. Middle graph was discarded because of a dissociation length  $>100$  nm, the maximum expected system stretching according to the known linker lengths. Bottom graph is characteristic of a short-range, nonelastic, unspecific tip-surface interaction.

$10^{-2} \pm 1.0 \times 10^{-2} \text{ s}^{-1}$ , and reaction lengths of  $x_B = 3.98 \pm 0.33$  and  $0.52 \pm 0.23 \text{ \AA}$ .

## DISCUSSION

DXS belongs to a subclass of TPP-dependent enzymes that combine characteristics of decarboxylases and transketolases. A reaction mechanism has been proposed (41) involving formation of a highly reactive TPP ylide, nucleophilic attack of the ylide on the donor substrate (pyruvate), elimination of the first product ( $\text{CO}_2$ ), nucleophilic attack of the  $\alpha$ -carbanion/enamine on the acceptor substrate (G3P), elimination of the second product (DXP), and regeneration of TPP. Our data obtained at single-molecule resolution confirm the sequentiality in the incorporation of both substrates into the active center, evidenced by the requirement of soluble pyruvate for maximal DXS-G3P binding but not of soluble G3P for maximal DXS-pyruvate interaction. Moreover,  $\text{CO}_2$  trapping experiments showed that DXS does not efficiently catalyze the decarboxylation of pyruvate and release of  $\text{CO}_2$  in the absence of G3P (41), indicating that the binding of G3P is required to form a catalytically competent complex. On the basis of these results, an ordered mechanism can be proposed where entry of pyruvate in the active center increases

the affinity of the enzyme for the second substrate, G3P, which is required for the catalysis to proceed. SMFS data indicate that the interaction of DXS with G3P and pyruvate remains unchanged regardless of the presence of TPP, in opposition to SPR assays where the cofactor is required for the retention of the enzyme on the substrate layer. These apparently contradictory results suggest that parameters derived from techniques that analyze molecular populations cannot be extrapolated directly to predict the behavior of individual molecules. Whereas biomolecules in conventional ensemble assays are interrogated simultaneously in large numbers and average properties are extracted, in single molecule experiments they are probed one at a time, gaining access to new types of information. The interaction of DXS with its substrates might be too brief in the absence of TPP to allow a measurable DXS layer deposition on the substrate-coated SPR chip, but long enough to be detected by SMFS as a brief binding event. In the case of pyruvate:



Our data lead us to propose that, in the absence of TPP, the transiently formed DXS-pyruvate complex quickly dissociates; whereas in the presence of TPP, the equilibrium is displaced toward a relatively stable species involving DXS, pyruvate, and TPP. Under adequate conditions, probably not met by crosslinked substrates, this ternary complex undergoes decarboxylation and is ready to transfer the acetyl group to G3P. In this scenario, the ternary complex DXS-pyruvate-TPP, but not the short-lived DXS-pyruvate species, might have a sufficiently low dissociation rate to allow for the formation of a significant molecular layer amenable to SPR detection. SMFS, however, could likely detect the presence of the labile DXS-pyruvate intermediate in a significant number of the 1-s cycles of each experiment. This finding highlights the potential of single-molecule analysis to unravel molecular phenomena that escape detection when studied by other techniques. The proposed stability of the ternary complex DXS-pyruvate-TPP would explain our SPR data where, after the

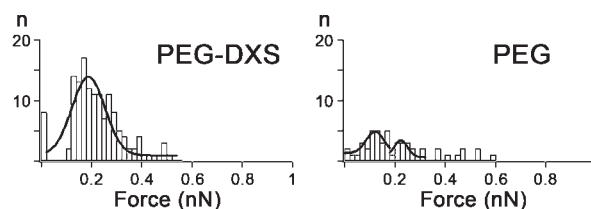


**Figure 7.** Control assay of the effect of the PEG linker on unspecific SMFS interactions. A pyruvate-coated surface was probed with cantilevers functionalized with PEG-DXS or only with PEG. Corresponding histograms were fitted to gaussian curves.

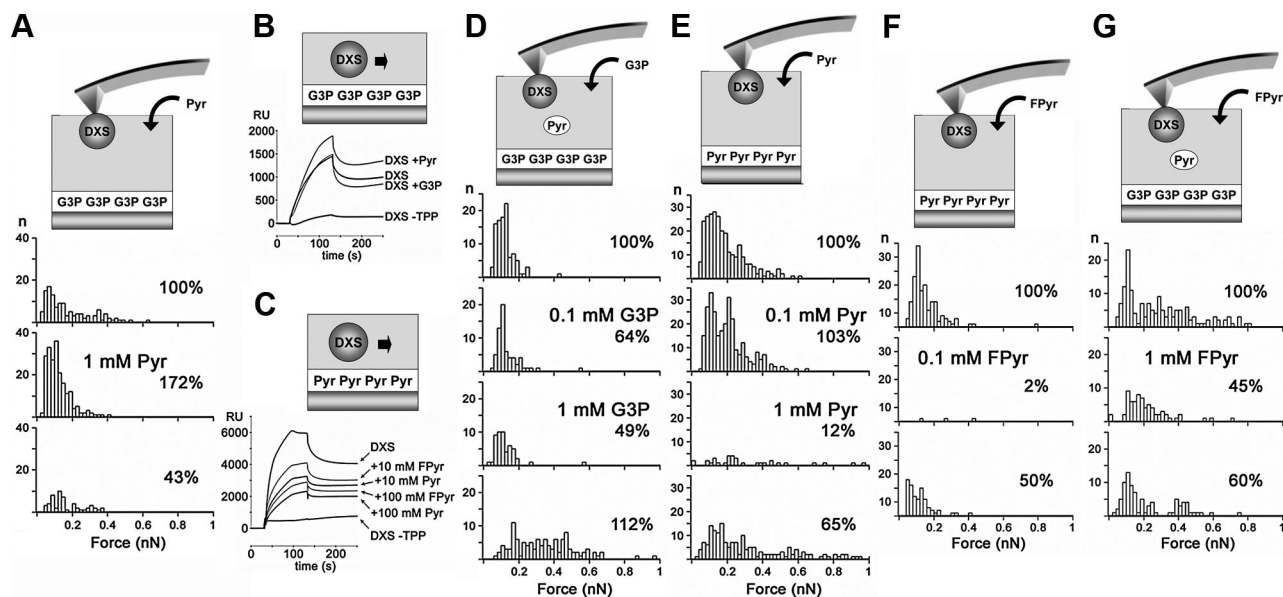


**Figure 8.** Analysis of the interaction of DXS with pyruvate and G3P in SMFS assays. *A)* SMFS analysis of the effect of soluble pyruvate on the interaction between immobilized DXS and G3P. Percentages represent frequency of binding events in the different experimental configurations. Temporal sequence from top to bottom: no soluble pyruvate, addition of 1 mM pyruvate, removal of soluble pyruvate. *B)* Effect of the presence of soluble TPP, G3P, and pyruvate on the SPR analysis of DXS binding to a G3P-coated chip. All samples contained 1 mM TPP, except DXS - TPP. *C)* SPR analysis of the effect of fluoropyruvate on the binding between DXS and pyruvate. All samples contained 1 mM TPP, except DXS - TPP. *D)* SMFS analysis of the effect of soluble G3P on the binding between immobilized DXS and G3P. All samples contained 1 mM pyruvate. Temporal sequence from top to bottom: no soluble G3P, addition of 0.1 mM G3P, addition of 1 mM G3P, removal of soluble G3P. *E)* SMFS analysis of the effect of soluble pyruvate on the binding between immobilized DXS and pyruvate. Temporal sequence from top to bottom: no soluble pyruvate, addition of 0.1 mM pyruvate, addition of 1 mM pyruvate, removal of soluble pyruvate. *F)* SMFS analysis of the effect of soluble fluoropyruvate on the binding between immobilized DXS and pyruvate. Temporal sequence from top to bottom: no soluble fluoropyruvate, addition of 0.1 mM fluoropyruvate, removal of soluble fluoropyruvate. *G)* SMFS analysis of the effect of soluble fluoropyruvate on the binding between immobilized DXS and G3P. All samples contained 1 mM pyruvate. Temporal sequence from top to bottom: no soluble fluoropyruvate, addition of 1 mM fluoropyruvate, removal of soluble fluoropyruvate.

association phase, rinsing the surface with buffer did not induce a rapid decrease of the signal. Maintenance of the interaction between DXS and tethered pyruvate, accounting for the sustained SPR signal, could result from a blockage in the reaction due to the presence of the linker in place of the pyruvate methyl group. Although the methyl group does not participate in the catalysis, the presence of a linker might introduce steric hindrances preventing progress of the reaction. The same reasoning can be applied to SPR results obtained with immobilized G3P.

One of the principal challenges of understanding enzyme catalysis is resolving the dynamics of enzyme-substrate interactions with ångström resolution, the length scale at which chemistry occurs (59). The two force regimes detected in DFS plots for the interaction DXS-pyruvate suggest the existence of a first step involving the formation of a relatively stable complex with a mean dissociation length of  $\sim 4$  Å, which might correspond to the initial recognition between the enzyme and its first substrate. A second, unstable, complex with a mean dissociation length  $< 1$  Å could reflect atomic interactions involved in bond formation. An interesting observation with regard to the future development of a nanosensor device is the ability of tethered DXS to efficiently bind its two substrates without having a very high catalytic activity. Current activity assays used to

detect inhibitors invariably need metabolically active enzymes, whereas the data presented here indicate that SMFS-based nanosensors might only require enzyme binding to the substrates, without the need for product synthesis. This finding suggests a dissociation of DXS activity between substrate recognition properties, which are retained by the tethered enzyme, and substrate transformation, which seemingly depends significantly on the presence of an intact enzyme. The strategy used to immobilize DXS on the AFM tip could have altered the chemical neighborhood of some key reactive groups, or it might have rendered the enzyme less free to adapt by induced fit to its substrates.

Enzyme inhibition is the major mechanism of action of many drugs, including antiinflammatory (60), antihypertensive (61), antineoplastic (62–65), antidepressant (66), antiasthmatic (67), anti-Parkinson (68), anti-Alzheimer (69–71), lipid-lowering (72), anti-AIDS (73,74), and antimicrobial compounds (4, 6, 7). The absence of the MEP pathway in animals suggests that inhibitors of its enzymes can be used at relatively high concentrations to treat certain bacterial and protozoan infections without exhibiting undesired side-effects. In addition, this will lead to a higher efficiency of the drug and, in turn, to a reduction in the appearance of resistant strains typically observed when a drug is administered at sublethal doses for an extended period. Microbes often can revert a blocked

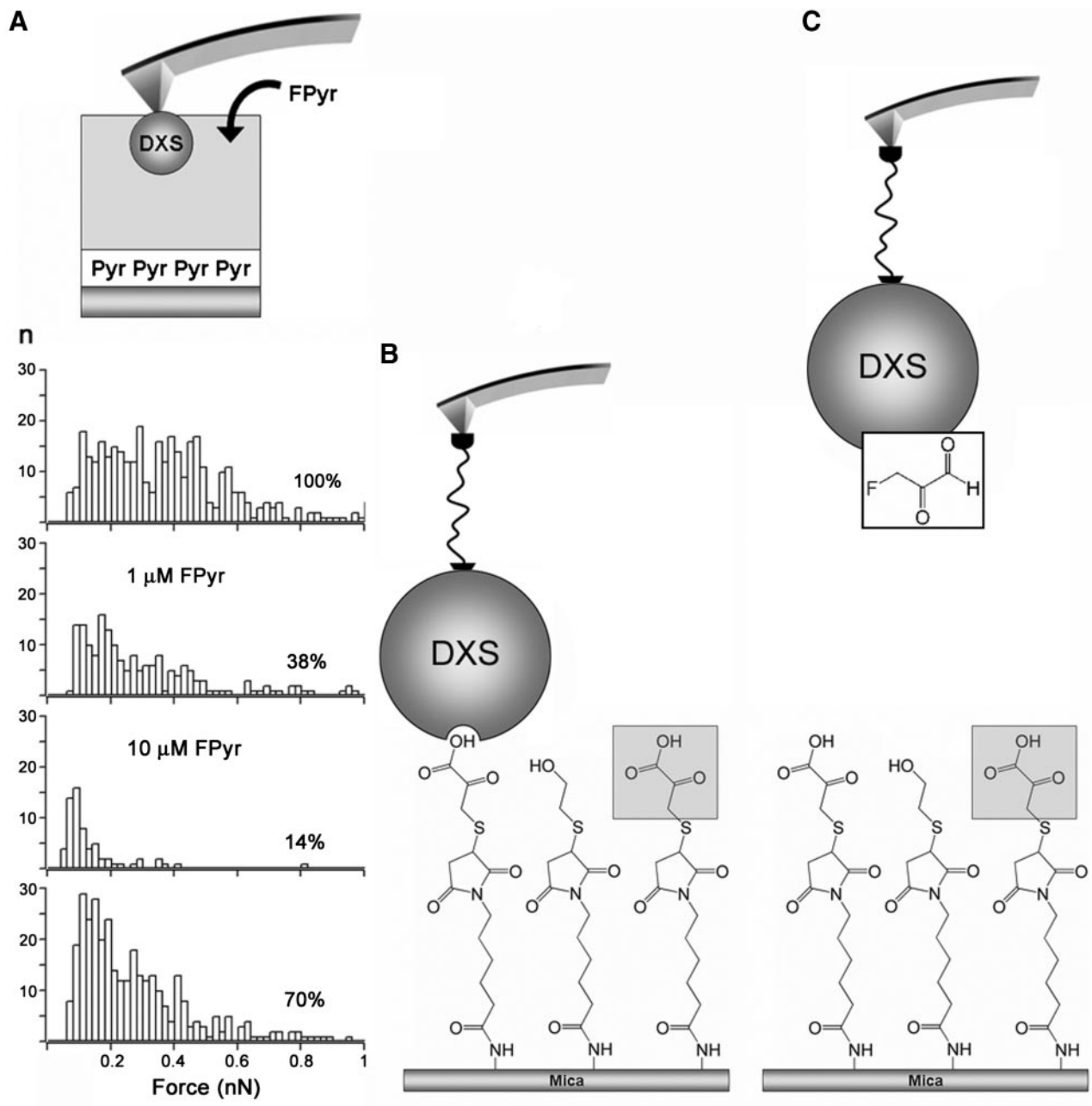


**Figure 9.** High-sensitivity single-molecule nanosensor for the detection of DXS inhibitors. *A*) SMFS analysis of the effect of soluble fluoropyruvate on the binding between immobilized DXS and pyruvate, using a DXS concentration 100 times smaller than that in Fig. 8*F*. Temporal sequence from top to bottom: no soluble fluoropyruvate, addition of 1  $\mu$ M fluoropyruvate, addition of 10  $\mu$ M fluoropyruvate, removal of soluble fluoropyruvate. *B*) Configuration showing the interaction between DXS bound to nanoscale sensor and pyruvate to mica surfaces. *C*) A significant decrease in the binding of DXS to the pyruvate-functionalized surface indicates the presence of an inhibitor in solution.

pathway through the recruitment of enzymatic activities that participate in similar reactions and that, by means of mutations that alter their substrate specificity or their expression levels, can metabolize alternative substrates into intermediaries located downstream of the blocked step. A second characteristic that makes the MEP pathway a particularly suitable target for the development of antibiotics derives from the observation that when its steps are blocked very low rates of reversion are observed (75). Fosmidomycin, an inhibitor of DXP reductoisomerase, the second enzyme of the MEP pathway, has shown

antimalarial activity *in vitro* and in murine malaria models (76), and early clinical studies have now proven its efficacy and safety in the treatment of uncomplicated *P. falciparum* malaria in humans (77). It can be foreseen that by selectively blocking other MEP pathway steps a similar effect to that observed for fosmidomycin will be found and that some of the compounds inhibiting these enzymes would also act on the parasite (7). In agreement with this view, the DXS inhibitor fluoropyruvate was proposed as a putative antimalarial drug (41).

Pyruvate, with a molecular mass of only 88 Da, is to

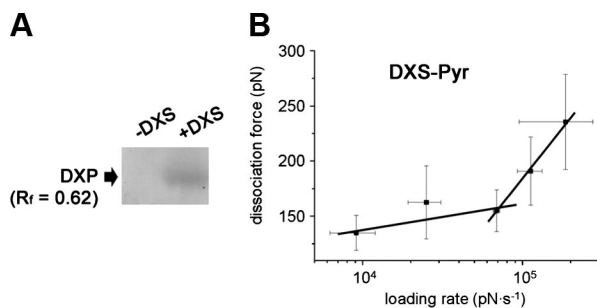


**Figure 10.** Calculation of enzymatic parameters. A) TLC analysis of the activity of DXS crosslinked to agarose beads. B) Dynamic force spectroscopy graph for the interaction between immobilized DXS and pyruvate in SMFS assays, where the measured dissociation forces are plotted against the loading rate.

date the smallest substrate that has been immobilized in an active form for its use in dynamic force spectroscopy assays, thus expanding the powerful applications of this technique to the study of the interactions of very small molecules. The strategy used to covalently cross-link G3P through its phosphate group into surfaces in a form adequate for recognition by its metabolizing enzyme opens the field to single-molecule analysis of similarly reactive phosphate-containing enzyme substrates. Using pyruvate as the immobilized substrate we could detect the presence of fluoropyruvate at lower concentrations than those required when using immobilized G3P, probably because of the requirement in the latter case of soluble pyruvate in solution, that will compete with the inhibitor for DXS binding (41). This, in addition to the tedious synthesis of the G3P derivative when compared with commercially available mercaptopyruvate, makes a pyruvate-based sensor the preferred configuration. The higher efficiency of fluoropyruvate relative to pyruvate in preventing DXS binding to its immobilized substrate likely reflects an increased residence time or the induction of conformational changes in the active center that might be related to the molecular mechanism of inhibition. This opens good perspectives regarding the application of SMFS-based nanosensors to the biodiscovery of novel enzyme inhibitors found in minute amounts. Enzymatic assays have established fluoropyruvate as a DXS competitive inhibitor with a  $K_i$  of 1 mM (41), whereas we have shown that an SMFS-based nanosensor can detect 10  $\mu$ M fluoropyruvate by using conventional experimental protocols and commercial AFM cantilevers. Considering that fluoropyruvate is a relatively weak DXS inhibitor, more active compounds (78) can presumably be discovered at concentrations within the nanomolar range using the SMFS approach presented here. We foresee that maximal resolution can be attained when nanofabrication methods will permit the functionalization of force nanosensors carrying a single enzyme molecule (Fig. 9B, C). Such future truly single-molecule devices will open the field for the coupling to very small scale synthesis of combinatorial chemical libraries and for the biodiscovery

of compounds represented only by a few dozens of molecules in the sensor chamber. EJ

This work was supported by grants BIO2002-00128, BIO2002-04419-C02-02, BIO2005-01591, BIO2008-01184, CSD2007-00036, and CSD2006-00012 from the Ministerio de Ciencia e Innovación, Spain, which included FEDER funds, and by grants 2009SGR-760, 2009SGR-0026, and 2005SGR-00914 from the Generalitat de Catalunya, Spain. We thank the Nanotechnology Platform of the Barcelona Scientific Park and Marta Taulés (Scientific and Technical Services of the University of Barcelona) for technical assistance.

## REFERENCES

- Palumbi, S. R. (2001) Humans as the world's greatest evolutionary force. *Science* **293**, 1786–1790
- Walsh, C. (2003) Where will new antibiotics come from? *Nat. Rev. Microbiol.* **1**, 65–70
- Beytia, E. D., and Porter, J. W. (1976) Biochemistry of polyisoprenoid biosynthesis. *Annu. Rev. Biochem.* **45**, 113–142
- Eisenreich, W., Rohdich, F., and Bacher, A. (2001) Deoxyxylulose phosphate pathway to terpenoids. *Trends Plant Sci.* **6**, 78–84
- Takahashi, S., Kuzuyama, T., Watanabe, H., and Seto, H. (1998) A 1-deoxy-D-xylulose 5-phosphate reductoisomerase catalyzing the formation of 2-C-methyl-D-erythritol 4-phosphate in an alternative nonmevalonate pathway for terpenoid biosynthesis. *Proc. Natl. Acad. Sci. U. S. A.* **95**, 9879–9884
- Rohdich, F., Kis, K., Bacher, A., and Eisenreich, W. (2001) The non-mevalonate pathway of isoprenoids: genes, enzymes and intermediates. *Curr. Opin. Chem. Biol.* **5**, 535–540
- Rodríguez-Concepción, M. (2004) The MEP pathway: a new target for the development of herbicides, antibiotics and antimalarial drugs. *Curr. Pharm. Des.* **10**, 2391–2400
- Jomaa, H., Wiesner, J., Sanderbrand, S., Altincicek, B., Weidemeyer, C., Hintz, M., Turbachova, I., Eberl, M., Zeidler, J., Lichtenthaler, H. K., Soldati, D., and Beck, E. (1999) Inhibitors of the nonmevalonate pathway of isoprenoid biosynthesis as antimalarial drugs. *Science* **285**, 1573–1576
- Ralph, S. A., D'Ombrain, M. C., and McFadden, G. I. (2001) The apicoplast as an antimalarial drug target. *Drug Resist. Updat.* **4**, 145–151
- Jain, K. K. (2005) The role of nanobiotechnology in drug discovery. *Drug Discov. Today* **10**, 1435–1442
- Santos-Magalhaes, N. S., and Mosqueira, V. C. (2010) Nanotechnology applied to the treatment of malaria. *Adv. Drug Deliv. Rev.* **62**, 560–575
- Bizzarri, A. R., and Cannistraro, S. (2010) The application of atomic force spectroscopy to the study of biological complexes undergoing a biorecognition process. *Chem. Soc. Rev.* **39**, 734–749
- Bustamante, C., Macosko, J. C., and Wuite, G. J. (2000) Grabbing the cat by the tail: manipulating molecules one by one. *Nat. Rev. Mol. Cell. Biol.* **1**, 130–136
- Evans, E., and Ritchie, K. (1997) Dynamic strength of molecular adhesion bonds. *Biophys. J.* **72**, 1541–1555
- Merkel, R., Nassoy, P., Leung, A., Ritchie, K., and Evans, E. (1999) Energy landscapes of receptor-ligand bonds explored with dynamic force spectroscopy. *Nature* **397**, 50–53
- Zlatanova, J., Lindsay, S. M., and Leuba, S. H. (2000) Single molecule force spectroscopy in biology using the atomic force microscope. *Prog. Biophys. Mol. Biol.* **74**, 37–61
- Perez-Jimenez, R., Li, J., Kosuri, P., Sanchez-Romero, I., Wiita, A. P., Rodriguez-Larrea, D., Chueca, A., Holmgren, A., Miranda-Vizuete, A., Becker, K., Cho, S. H., Beckwith, J., Gelhaye, E., Jacquot, J. P., Gaucher, E. A., Sanchez-Ruiz, J. M., Berne, B. J., and Fernandez, J. M. (2009) Diversity of chemical mechanisms in thioredoxin catalysis revealed by single-molecule force spectroscopy. *Nat. Struct. Mol. Biol.* **16**, 890–896
- Sletmoen, M., Skjak-Braek, G., and Stokke, B. T. (2005) Mapping enzymatic functionalities of mannuronan C-5 epimerases and their modular units by dynamic force spectroscopy. *Carbohydr. Res.* **340**, 2782–2795

19. Wiita, A. P., Perez-Jimenez, R., Walther, K. A., Gräter, F., Berne, B. J., Holmgren, A., Sanchez-Ruiz, J. M., and Fernandez, J. M. (2007) Probing the chemistry of thioredoxin catalysis with force. *Nature* **450**, 124–127
20. Yingge, Z., Chunli, B., Chen, W., and Delu, Z. (2001) Force spectroscopy between acetylcholine and single acetylcholinesterase molecules and the effects of inhibitors and reactivators studied by atomic force microscopy. *J. Pharmacol. Exp. Ther.* **297**, 798–803
21. Fiorini, M., McKendry, R., Cooper, M. A., Rayment, T., and Abell, C. (2001) Chemical force microscopy with active enzymes. *Biophys. J.* **80**, 2471–2476
22. Kamper, S. G., Porter-Peden, L., Blankespoor, R., Sinniah, K., Zhou, D., Abell, C., and Rayment, T. (2007) Investigating the specific interactions between carbonic anhydrase and a sulfonamide inhibitor by single-molecule force spectroscopy. *Langmuir* **23**, 12561–12565
23. Porter-Peden, L., Kamper, S. G., Wal, M. V., Blankespoor, R., and Sinniah, K. (2008) Estimating kinetic and thermodynamic parameters from single molecule enzyme-inhibitor interactions. *Langmuir* **24**, 11556–11561
24. Maki, T., Kidoaki, S., Usui, K., Suzuki, H., Ito, M., Ito, F., Hayashizaki, Y., and Matsuda, T. (2007) Dynamic force spectroscopy of the specific interaction between the PDZ domain and its recognition peptides. *Langmuir* **23**, 2668–2673
25. Evans, E., Leung, A., Heinrich, V., and Zhu, C. (2004) Mechanical switching and coupling between two dissociation pathways in a P-selectin adhesion bond. *Proc. Natl. Acad. Sci. U. S. A.* **101**, 11281–11286
26. Funari, G., Domenici, F., Nardinocchi, L., Puca, R., D'Orazi, G., Bizzarri, A. R., and Cannistraro, S. (2010) Interaction of p53 with Mdm2 and azurin as studied by atomic force spectroscopy. *J. Mol. Recogn.* **23**, 343–351
27. Taranta, M., Bizzarri, A. R., and Cannistraro, S. (2008) Probing the interaction between p53 and the bacterial protein azurin by single molecule force spectroscopy. *J. Mol. Recognit.* **21**, 63–70
28. Rico, F., and Moy, V. T. (2007) Energy landscape roughness of the streptavidin-biotin interaction. *J. Mol. Recognit.* **20**, 495–501
29. Neuert, G., Albrecht, C., Pamir, E., and Gaub, H. E. (2006) Dynamic force spectroscopy of the digoxigenin-antibody complex. *FEBS Lett.* **580**, 505–509
30. Allen, S., Chen, X., Davies, J., Davies, M. C., Dawkes, A. C., Edwards, J. C., Roberts, C. J., Sefton, J., Tendler, S. J., and Williams, P. M. (1997) Detection of antigen-antibody binding events with the atomic force microscope. *Biochemistry* **36**, 7457–7463
31. Schwesinger, F., Ros, R., Strunz, T., Anselmetti, D., Güntherodt, H. J., Honegger, A., Jeremut, L., Tiefenauer, L., and Pluckthun, A. (2000) Unbinding forces of single antibody-antigen complexes correlate with their thermal dissociation rates. *Proc. Natl. Acad. Sci. U. S. A.* **97**, 9972–9977
32. Hinterdorfer, P., Baumgartner, W., Gruber, H. J., Schilcher, K., and Schindler, H. (1996) Detection and localization of individual antibody-antigen recognition events by atomic force microscopy. *Proc. Natl. Acad. Sci. U. S. A.* **93**, 3477–3481
33. Bartels, F. W., Baumgarth, B., Anselmetti, D., Ros, R., and Becker, A. (2003) Specific binding of the regulatory protein ExpG to promoter regions of the galactoglucan biosynthesis gene cluster of *Sinorhizobium meliloti*—a combined molecular biology and force spectroscopy investigation. *J. Struct. Biol.* **143**, 145–152
34. Kühner, F., Costa, L. T., Bisch, P. M., Thalhammer, S., Heckl, W. M., and Gaub, H. E. (2004) LexA-DNA bond strength by single molecule force spectroscopy. *Biophys. J.* **87**, 2683–2690
35. Bonanni, B., Bizzarri, A. R., and Cannistraro, S. (2006) Optimized biorecognition of cytochrome *c* 551 and azurin immobilized on thiol-terminated monolayers assembled on Au(111) substrates. *J. Phys. Chem. B* **110**, 14574–14580
36. Garcia-Manyes, S., Bucior, I., Ros, R., Anselmetti, D., Sanz, F., Burger, M. M., and Fernández-Busquets, X. (2006) Proteoglycan mechanics studied by single-molecule force spectroscopy of allotypic cell adhesion glycans. *J. Biol. Chem.* **281**, 5992–5999
37. Anselmetti, D., Fritz, J., Smith, B., and Fernández-Busquets, X. (2000) Single molecule DNA biophysics with atomic force microscopy. *Single Mol.* **1**, 53–58
38. Meadows, P. Y., Bemis, J. E., and Walker, G. C. (2003) Single-molecule force spectroscopy of isolated and aggregated fibronectin proteins on negatively charged surfaces in aqueous liquids. *Langmuir* **19**, 9566–9572
39. Rief, M., and Grubmüller, H. (2002) Force spectroscopy of single biomolecules. *Chemphyschem* **3**, 255–261
40. Green, J. B. D., Novoradovsky, A., Park, D., and Lee, G. U. (1999) Microfabricated tip arrays for improving force measurements. *Appl. Phys. Lett.* **74**, 1489–1491
41. Eubanks, L. M., and Poulter, C. D. (2003) Rhodobacter capsulatus 1-deoxy-D-xylulose 5-phosphate synthase: steady-state kinetics and substrate binding. *Biochemistry* **42**, 1140–1149
42. Hibbert, H., and Whelen, M. S. (1929) Studies on reactions relating to carbohydrates and polysaccharides. XXIII. Synthesis and properties of hydroxy alkylidene glycols and glycerols. *J. Am. Chem. Soc.* **51**, 3115–3123
43. Wilkinson, T. A., Yin, J., Pidgeon, C., and Post, C. B. (2000) Alkylation of cysteine-containing peptides to mimic palmitoylation. *J. Peptide. Res.* **55**, 140–147
44. Querol, J., Rodríguez-Concepción, M., Boronat, A., and Imperial, S. (2001) Essential role of residue H49 for activity of *Escherichia coli* 1-deoxy-D-xylulose 5-phosphate synthase, the enzyme catalyzing the first step of the 2-C-methyl-D-erythritol 4-phosphate pathway for isoprenoid synthesis. *Biochem. Biophys. Res. Commun.* **289**, 155–160
45. Bradford, M. M. (1976) A rapid and sensitive method for the quantitation of microgram quantities of protein utilizing the principle of protein-dye binding. *Anal. Biochem.* **72**, 248–254
46. Lyubchenko, Y., Shlyakhtenko, L., Harrington, R., Oden, P., and Lindsay, S. (1993) Atomic force microscopy of long DNA: imaging in air and under water. *Proc. Natl. Acad. Sci. U. S. A.* **90**, 2137–2140
47. Hegner, M., Wagner, P., and Semenza, G. (1993) Ultralarge atomically flat template-stripped Au surfaces for scanning probe microscopy. *Surf. Sci.* **291**, 39–46
48. Frey, B. L., and Corn, R. M. (1996) Covalent attachment and derivatization of poly(L-lysine) monolayers on gold surfaces as characterized by polarization-modulation FT-IR spectroscopy. *Anal. Chem.* **68**, 3187–3193
49. Altincicek, B., Hintz, M., Sanderbrand, S., Wiesner, J., Beck, E., and Jomaa, H. (2000) Tools for discovery of inhibitors of the 1-deoxy-D-xylulose 5-phosphate (DXP) synthase and DXP reductoisomerase: an approach with enzymes from the pathogenic bacterium *Pseudomonas aeruginosa*. *FEMS Microbiol. Lett.* **190**, 329–333
50. Hoeffler, J. F., Tritsch, D., Grosdemange-Billiard, C., and Rohmer, M. (2002) Isoprenoid biosynthesis via the methylerythritol phosphate pathway. Mechanistic investigations of the 1-deoxy-D-xylulose 5-phosphate reductoisomerase. *Eur. J. Biochem.* **269**, 4446–4457
51. Lois, L. M., Campos, N., Putra, S. R., Danielsen, K., Rohmer, M., and Boronat, A. (1998) Cloning and characterization of a gene from *Escherichia coli* encoding a transketolase-like enzyme that catalyzes the synthesis of D-1-deoxyxylulose 5-phosphate, a common precursor for isoprenoid, thiamin, and pyridoxol biosynthesis. *Proc. Natl. Acad. Sci. U. S. A.* **95**, 2105–2110
52. Florin, E. L., Rief, M., Lehmann, H., Ludwig, M., Dornmair, C., Moy, V. T., and Gaub, H. E. (1995) Sensing specific molecular interactions with the atomic force microscope. *Biosens. Bioelectron.* **10**, 895–901
53. Eckel, R., Wilking, S. D., Becker, A., Sewald, N., Ros, R., and Anselmetti, D. (2005) Single-molecule experiments in synthetic biology: an approach to the affinity ranking of DNA-binding peptides. *Angew. Chem. Int. Ed. Engl.* **44**, 3921–3924
54. Xiang, S., Usunow, G., Lange, G., Busch, M., and Tong, L. (2007) Crystal structure of 1-deoxy-D-xylulose 5-phosphate synthase, a crucial enzyme for isoprenoids biosynthesis. *J. Biol. Chem.* **282**, 2676–2682
55. Schürmann, M., Schürmann, M., and Sprenger, G. A. (2002) Fructose 6-phosphate aldolase and 1-deoxy-D-xylulose 5-phosphate synthase from *Escherichia coli* as tools in enzymatic synthesis of 1-deoxysugars. *J. Mol. Catal. B* **19–20**, 247–252
56. Sodhi, R. N. (2004) Time-of-flight secondary ion mass spectrometry (TOF-SIMS): versatility in chemical and imaging surface analysis. *Analyst* **129**, 483–487
57. Myszka, D. G. (1997) Kinetic analysis of macromolecular interactions using surface plasmon resonance biosensors. *Curr. Opin. Biotechnol.* **8**, 50–57

58. Schürmann, M. (2001) *1-Deoxy-D-xylulose-5-phosphat Synthase von Escherichia coli: biochemische Charakterisierung und Struktur-Funktionsbeziehungen*. Ph.D. thesis, Universität Düsseldorf
59. Kraut, D. A., Carroll, K. S., and Herschlag, D. (2003) Challenges in enzyme mechanism and energetics. *Annu. Rev. Biochem.* **72**, 517–571
60. Vane, J. R., and Botting, R. M. (1998) Anti-inflammatory drugs and their mechanism of action. *Inflamm. Res.* **47**(Suppl. 2), S78–S87
61. Menard, J., and Patchett, A. A. (2001) Angiotensin-converting enzyme inhibitors. *Adv. Protein Chem.* **56**, 13–75
62. Prendergast, G. C., and Oliff, A. (2000) Farnesyltransferase inhibitors: antineoplastic properties, mechanisms of action, and clinical prospects. *Semin. Cancer Biol.* **10**, 443–452
63. Kaubisch, A., and Schwartz, G. K. (2000) Cyclin-dependent kinase and protein kinase C inhibitors: a novel class of antineoplastic agents in clinical development. *Cancer J.* **6**, 192–212
64. Mathijssen, R. H., Loos, W. J., Verweij, J., and Sparreboom, A. (2002) Pharmacology of topoisomerase I inhibitors irinotecan (CPT-11) and topotecan. *Curr. Cancer Drug Targets* **2**, 103–123
65. Simpson, E. R., and Dowsett, M. (2002) Aromatase and its inhibitors: significance for breast cancer therapy. *Recent. Prog. Horm. Res.* **57**, 317–338
66. Finberg, J. P. (1995) Pharmacology of reversible and selective inhibitors of monoamine oxidase type A. *Acta Psychiatr. Scand. Suppl.* **386**, 8–13
67. Schmidt, D., Dent, G., and Rabe, K. F. (1999) Selective phosphodiesterase inhibitors for the treatment of bronchial asthma and chronic obstructive pulmonary disease. *Clin. Exp. Allergy* **29**(Suppl. 2), 99–109
68. Olanow, C. W. (1993) MAO-B inhibitors in Parkinson's disease. *Adv. Neurol.* **60**, 666–671
69. Thomas, T. (2000) Monoamine oxidase-B inhibitors in the treatment of Alzheimer's disease. *Neurobiol. Aging* **21**, 343–348
70. Frisoni, G. B. (2001) Treatment of Alzheimer's disease with acetylcholinesterase inhibitors: bridging the gap between evidence and practice. *J. Neurol.* **248**, 551–557
71. Ghosh, A. K., Hong, L., and Tang, J. (2002)  $\beta$ -secretase as a therapeutic target for inhibitor drugs. *Curr. Med. Chem.* **9**, 1135–1144
72. Moghadasian, M. H. (1999) Clinical pharmacology of 3-hydroxy-3-methylglutaryl coenzyme A reductase inhibitors. *Life Sci.* **65**, 1329–1337
73. Lebon, F., and Ledecq, M. (2000) Approaches to the design of effective HIV-1 protease inhibitors. *Curr. Med. Chem.* **7**, 455–477
74. Nair, V. (2002) HIV integrase as a target for antiviral chemotherapy. *Rev. Med. Virol.* **12**, 179–193
75. Sauret-Güeto, S., Urós, E. M., Ibáñez, E., Boronat, A., and Rodríguez-Concepción, M. (2006) A mutant pyruvate dehydrogenase E1 subunit allows survival of *Escherichia coli* strains defective in 1-deoxy-D-xylulose 5-phosphate synthase. *FEBS Lett.* **580**, 736–740
76. Wiesner, J., Borrmann, S., and Jomaa, H. (2003) Fosmidomycin for the treatment of malaria. *Parasitol. Res.* **90**(Suppl. 2), S71–S76
77. Borrmann, S., Lundgren, I., Oyakhirome, S., Impouma, B., Matsiegui, P. B., Adegnika, A. A., Issifou, S., Kun, J. F. J., Hutchinson, D., Wiesner, J., Jomaa, H., and Kremsner, P. G. (2006) Fosmidomycin plus clindamycin for treatment of pediatric patients aged 1 to 14 years with *Plasmodium falciparum* malaria. *Antimicrob. Agents Chemother.* **50**, 2713–2718
78. Mao, J., Eoh, H., He, R., Wang, Y., Wan, B., Franzblau, S. G., Crick, D. C., and Kozikowski, A. P. (2008) Structure-activity relationships of compounds targeting *Mycobacterium tuberculosis* 1-deoxy-D-xylulose 5-phosphate synthase. *Bioorg. Med. Chem. Lett.* **18**, 5320–5323

Received for publication February 11, 2010.

Accepted for publication June 24, 2010.